sound in a Bose–Einstein condensate. Under these conditions we expect phonon excitation during light pulse propagation through the condensate. By deliberately tuning another laser beam to the $|2\rangle \rightarrow |4\rangle$ transition, it should be possible to demonstrate optical switching at the single photon level[24]. Finally, we note that during propagation of the atom clouds, light pulses are compressed in the z direction by a ratio of c/v_g. For our experimental parameters, that results in pulses with a spatial extent of only 43 μm. □

Received 3 November; accepted 21 December 1998.

1. Knight, P. L., Stoicheff, B. & Walls, D. (eds) Highlights in quantum optics. *Phil. Trans. R. Soc. Lond. A* **355,** 2215–2416 (1997).
2. Harris, S. E. Electromagnetically induced transparency. *Phys. Today* **50(7),** 36–42 (1997).
3. Scully, M. O. & Zubairy, M. S. *Quantum Optics* (Cambridge Univ. Press, 1997).
4. Arimondo, E. in *Progress in Optics* (ed. Wolf, E.) 257–354 (Elsevier Science, Amsterdam, 1996).
5. Bergmann, K., Theuer, H. & Shore, B. W. Coherent population transfer among quantum states of atoms and molecules. *Rev. Mod. Phys.* **70,** 1003–1006 (1998).
6. Chu, S. The manipulation of neutral particles. *Rev. Mod. Phys.* **70,** 685–706 (1998).
7. Cohen-Tannoudjii, C. N. Manipulating atoms with photons. *Rev. Mod. Phys.* **70,** 707–719 (1998).
8. Phillips, W. D. Laser cooling and trapping of neutral atoms. *Rev. Mod. Phys.* **70,** 721–741 (1998).
9. Hess, H. F. Evaporative cooling of magnetically trapped and compressed spin-polarized hydrogen. *Phys. Rev. B* **34,** 3476–3479 (1986).
10. Masuhara, N. *et al.* Evaporative cooling of spin-polarized atomic hydrogen. *Phys. Rev. Lett.* **61,** 935–938 (1988).
11. Anderson, M. H., Ensher, J. R., Matthews, M. R., Wieman, C. E. & Cornell, E. A. Observation of Bose-Einstein condensation in a dilute atomic vapor. *Science* **269,** 198–201 (1995).
12. Davis, K. B. *et al.* Bose-Einstein condensation in a gas of sodium atoms. *Phys. Rev. Lett.* **75,** 3969–3973 (1995).
13. Bradley, C. C., Sackett, C. A. & Hulet, R. G. Bose-Einstein condensation of lithium: observation of limited condensate number. *Phys. Rev. Lett.* **78,** 985–989 (1997).
14. Hau, L. V. *et al.* Near-resonant spatial images of confined Bose-Einstein condensates in a 4-Dee magnetic bottle. *Phys. Rev. A* **58,** R54–R57 (1998).
15. Hau, L. V., Golovchenko, J. A. & Burns, M. M. A new atomic beam source: The "candlestick". *Rev. Sci. Instrum.* **65,** 3746–3750 (1994).
16. Harris, S. E., Field, J. E. & Kasapi, A. Dispersive properties of electromagnetically induced transparency. *Phys. Rev. A* **46,** R29–R32 (1992).
17. Grobe, R., Hioe, F. T. & Eberly, J. H. Formation of shape-preserving pulses in a nonlinear adiabatically integrable system. *Phys. Rev. Lett.* **73,** 3183–3186 (1994).
18. Xiao, M., Li, Y.-Q., Jin, S.-Z. & Gea-Banacloche, J. Measurement of dispersive properties of electromagnetically induced transparency in rubidium atoms. *Phys. Rev. Lett.* **74,** 666–669 (1995).
19. Kasapi, A., Jain, M., Yin, G. Y. & Harris, S. E. Electromagnetically induced transparency: propagation dynamics. *Phys. Rev. Lett.* **74,** 2447–2450 (1995).
20. Schmidt, H. & Imamoglu, A. Giant Kerr nonlinearities obtained by electromagnetically induced transparency. *Opt. Lett.* **21,** 1936–1938 (1996).
21. Lambrecht, A., Courty, J. M., Reynaud, S. & Giacobino, E. Cold atoms: A new medium for quantum optics. *Appl. Phys. B* **60,** 129–134 (1995).
22. Hall, D. S., Matthews, M. R., Wieman, C. E. & Cornell, E. A. Measurements of relative phase in two-component Bose-Einstein condensates. *Phys. Rev. Lett.* **81,** 1543–1546 (1998).
23. Ruostekoski, J. & Walls, D. F. Coherent population trapping of Bose-Einstein condensates: detection of phase diffusion. *Eur. Phys. J. D* (submitted).
24. Harris, S. E. & Yamamoto, Y. Photon switching by quantum interference. *Phys. Rev. Lett.* **81,** 3611–3614 (1998).

Acknowledgements. We thank J. A. Golovchenko for discussions and C. Liu for experimental assistance. L.V.H. acknowledges support from the Rowland Institute for Science. S.E.H. is supported by the US Air Force Office of Scientific Research, the US Army Research Office, and the US Office of Naval Research. C.H.B. is supported by an NSF fellowship.

Correspondence and requests for materials should be addressed to L.V.H. (e-mail: hau@rowland.org).

Luttinger-liquid behaviour in carbon nanotubes

Marc Bockrath*, David H. Cobden*, Jia Lu*, Andrew G. Rinzler†, Richard E. Smalley†, Leon Balents‡ & Paul L. McEuen*

** Department of Physics, University of California and Materials Sciences Division, Lawrence Berkeley National Laboratory, Berkeley, California 94720, USA*
† Center for Nanoscale Science and Technology, Rice Quantum Institute and Department of Chemistry and Physics, MS-100, Rice University, PO Box 1892, Houston, Texas 77251, USA
‡ Institute for Theoretical Physics, University of California, Santa Barbara, California 93106-4030, USA

Electron transport in conductors is usually well described by Fermi-liquid theory, which assumes that the energy states of the electrons near the Fermi level E_F are not qualitatively altered by Coulomb interactions. In one-dimensional systems, however, even weak Coulomb interactions cause strong perturbations. The resulting system, known as a Luttinger liquid, is predicted to be distinctly different from its two- and three-dimensional counterparts[1]. For example, tunnelling into a Luttinger liquid at energies near the Fermi level is predicted to be strongly suppressed, unlike in two- and three-dimensional metals. Experiments on one-dimensional semiconductor wires[2,3] have been interpreted by using Luttinger-liquid theory, but an unequivocal verification of the theoretical predictions has not yet been obtained. Similarly, the edge excitations seen in fractional quantum Hall conductors are consistent with Luttinger-liquid behaviour[4,5], but recent experiments failed to confirm the predicted relationship between the electrical properties of the bulk state and those of the edge states[6]. Electrically conducting single-walled carbon nanotubes (SWNTs) represent quantum wires[7–10] that may exhibit Luttinger-liquid behaviour[11,12]. Here we present measurements of the conductance of bundles ('ropes') of SWNTs as a function of temperature and voltage that agree with predictions for tunnelling into a Luttinger liquid. In particular, we find that the conductance and differential conductance scale as power laws with respect to temperature and bias voltage, respectively, and that the functional forms and the exponents are in good agreement with theoretical predictions.

SWNTs are sufficiently robust and long to allow electrical connections to lithographically defined metallic electrodes, thereby making it possible to probe the intriguing electrical properties of

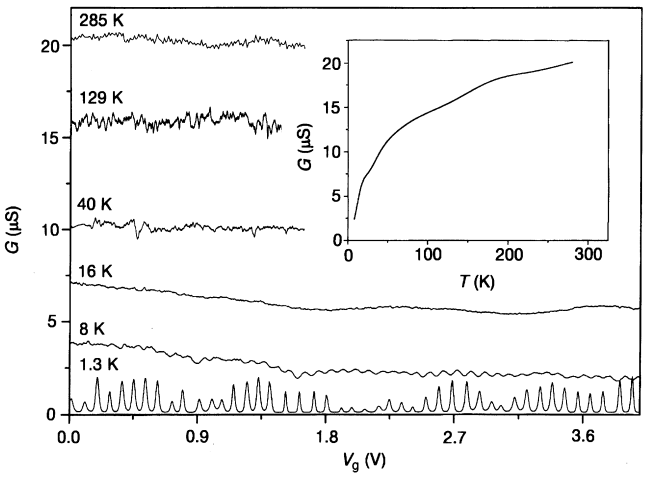

Figure 1 The two-terminal linear-response conductance G versus gate voltage V_g for a bulk-contacted metallic nanotube rope at a variety of temperatures. The data show significant temperature dependence for energy scales above the charging energy that cannot be explained by the Coulomb blockade model. Inset: average conductance as a function of temperature T. The samples used in these experiments are made in one of two ways. In both methods, SWNTs are deposited from a suspension in dichloroethane onto a 1-μm-thick layer of SiO_2 that has been thermally grown on a degenerately doped Si wafer, used as a gate electrode. Atomic force microscopy imaging reveals that the diameters of the ropes vary between 1 and 10 nm. In the first method[9], chromium–gold contacts are applied over the top of the nanotube rope using electron beam lithography and lift-off. From measurements of these devices in the Coulomb blockade regime, we conclude that the electrons are confined to the length of rope between the leads. This implies that the leads cut the nanotubes into segments, and transport involves tunnelling into the ends of the nanotubes ('end-contacted'). In the second method[10], electron-beam lithography is first used to define leads, and ropes are deposited on top of the leads. Samples were selected that showed Coulomb blockade behaviour at low temperatures with a single well-defined period, indicating the presence of a single quantum dot. The charging energy of these samples indicates a quantum dot with a size substantially larger than the spacing between the leads, as found by Tans *et al.*[10]. Transport thus occurs by electrons tunnelling into the middle, or bulk, of the nanotubes ('bulk-contacted').

these nanometre-sized structures[7–10,13,14]. Individual tubes, for example, are either semiconducting or conducting, depending on their chirality[7,8], whereas electron transport through ropes is typically dominated by a single metallic nanotube within the rope[9]. The latter observation is in agreement with the finding that most of the nanotubes in a rope are semiconductors and thus insulating at the low temperatures of transport measurements[7,8].

Electrical connections to nanotubes and nanotube ropes can be achieved by either depositing electrode metal over the top of the tubes ('end-contacted' samples), or by placing the tubes on top of predefined metal leads ('bulk-contacted' samples). We use both geometries to study the transport properties of nanotube ropes. Figure 1 gives an example of the measured two-terminal conductance, G, as a function of gate voltage, V_g, for a bulk-contacted metallic rope at different temperatures. The Coulomb oscillations[15] that occur each time an electron is added to a nanotube within the rope are clearly visible at low temperatures. The temperature dependence of the oscillations yields a charging energy U for this sample of 1.9 meV. At temperatures above 20 K, the thermal energy exceeds the charging energy (that is, $k_BT > U$, where k_B is Boltzmann's constant and T the absolute temperature). This results in the Coulomb oscillations being nearly completely 'washed out', rendering the conductance independent of gate voltage. The dependence on temperature is illustrated in Fig. 1 inset, which shows the conductance dropping steeply as the temperature is lowered, extrapolating to $G = 0$ at $T = 0$.

Figure 2 shows G as a function of T on a double logarithmic scale for two bulk-contacted and two end-contacted nanotube ropes (Fig. 2a and b, respectively). The measured data (solid lines) show approximate power-law behaviour, $G \propto T^{\alpha}$, for the four samples shown. However, the range of temperature over which this behaviour occurs is limited by the effects of Coulomb blockade at low temperatures. After correcting for the known temperature dependence due to the Coulomb blockade[15], the corrected data (dashed lines) show power-law behaviour over a greater temperature range, with slightly different exponents. Above $T \approx 100$ K, G begins to saturate for some samples. This saturation is observed in many, but not all, of the samples studied.

The corrected data obtained for the bulk-contacted samples show approximate power-law behaviour from 8 to 300 K with exponents $\alpha_{bulk} \approx 0.33$ and 0.38. In the case of the end-contacted samples, the corrected data show approximate power-law behaviour from 10 to 100 K with exponents $\alpha_{end} \approx 0.6$ for both samples. The upper inset to Fig. 2a shows the exponents determined from the temperature dependence of a variety of samples. Exponents marked with 'x' and 'o' are for bulk- and end-contacted tubes, respectively. The former show a systematically lower exponent than the latter samples with $\alpha_{end} \approx 0.6$ and $\alpha_{bulk} \approx 0.3$.

The two insets in Fig. 3 show the measured differential conductance dI/dV as a function of the applied bias voltage V. The upper inset in Fig. 3a shows results for a bulk-contacted sample (see lower inset) at different temperatures, plotted on a log–log scale. In linear response, dI/dV is proportional to a (temperature-dependent) constant, $G(T)$ from Fig. 2. At high biases, dI/dV increases with increasing V. The curves at different temperatures fall onto a single curve in the high-bias regime. As this curve is roughly linear on a log–log plot, it implies that the differential conductance is described by a power law, $dI/dV \propto V^{\alpha}$, where $\alpha = 0.36$. At the lowest temperature $T = 1.6$ K, this power-law behaviour occurs over two decades in V, from 1 to 100 mV.

The upper inset in Fig. 3b shows dI/dV as a function of V for an end-contacted sample (see lower inset) at several temperatures. The conductance is again a temperature-dependent constant at low biases $eV \ll k_BT$, whereas at higher biases dI/dV increases. The

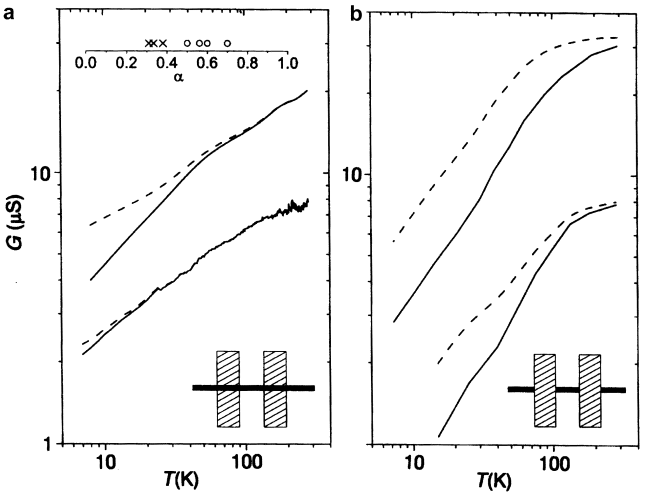

Figure 2 Conductance G plotted against temperature T for individual nanotube ropes. The data are plotted on a log–log scale. **a**, Data for ropes that are deposited over pre-defined leads (bulk-contacted); **b**, data for ropes that are contacted by evaporating the leads on top of the ropes (end-contacted). Sketches depicting the measurement configuration are shown in the lower insets. The plots show both the raw data (solid line) and the data corrected for the temperature dependence expected from the Coulomb blockade (CB) model (dashed line). We correct the data by dividing the measured $G(T)$ by the theoretically expected temperature dependence in the CB model. This correction factor depends only on U/k_BT, and, because U can be independently measured from the temperature dependence of the Coulomb oscillations, the correction procedure requires no adjustable parameters. If the CB were the only source of the temperature dependence, the dashed lines would be horizontal. Instead they have a finite slope, indicating an approximate power-law dependence on T. The upper inset to **a** shows the power-law exponents inferred for a variety of samples. Open circles denote end-contacted samples, and crosses denote bulk-contacted ones.

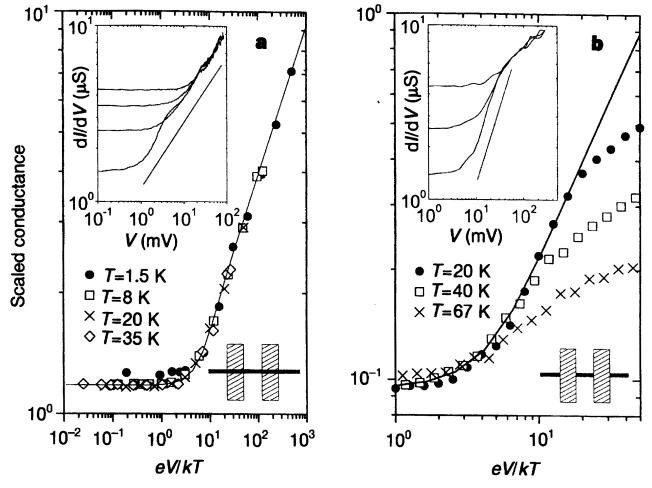

Figure 3 The differential conductance dI/dV measured at various temperatures. Inset in **a**, dI/dV curves taken on a bulk-contacted rope at temperatures $T = 1.6$ K, 8 K, 20 K and 35 K. Inset in **b**, dI/dV curves taken on an end-contacted rope at temperatures $T = 20$ K, 40 K and 67 K. In both insets, a straight line on the log–log plot is shown as a guide to the eye to indicate power-law behaviour. The main panels **a** and **b** show these measurements collapsed onto a single curve by using the scaling relations described in the text. The solid line is the theoretical result fitted to the data by using γ as a fitting parameter. The values of γ resulting in the best fit to the data are $\gamma = 0.46$ in **a** and $\gamma = 0.63$ in **b**.

high-bias data follows an approximate power law before rolling off to a reduced slope for $V > 30$ mV. Although the range of data is too small to conclude that a power law accurately describes the behaviour at intermediate voltages, if a straight line is fitted to the range $9\,\text{mV} < V < 32\,\text{mV}$, the exponent obtained is $\alpha = 0.87$.

A possible explanation for the approximate power-law behaviour that we see in our data is a strong energy dependence of the tunnel barrier, with increased tunnelling efficiency at high energies. This would lead to activated transport over the barrier, so that the conductance can be described by $G \propto \exp(-V_b/k_BT)$, where V_b is the height of the tunnel barriers. However, this general expression for G is inconsistent with our finding that the conductance extrapolates to $G = 0$ at $T = 0$ (Fig. 1 inset). The type of power-law behaviour that we observe could also arise if the electron transport were to occur through multiple quantum dots in series. Multiple quantum dots can be formed by disorder[16] or by barriers produced when the nanotubes bend over the lithographically defined contacts[17]. But as we have chosen to study only nanotube ropes that exhibit a single dominant period for the Coulomb oscillations at low temperatures, our samples are likely to contain only a single quantum dot.

A third possible explanation for the experimental observations would be that the nanotube ropes behave as a Luttinger liquid (LL). An LL is a one-dimensional correlated electron state characterized by a parameter g that measures the strength of the interaction between electrons. Strong repulsive interactions are characterized by $g \ll 1$, whereas $g = 1$ for the non-interacting electron gas. However, for any $g \neq 1$, the low-energy excitations of the system are not all weakly interacting quasiparticles, and the Fermi liquid theory used to describe conventional metals is not appropriate.

In SWNTs, the long-range Coulomb interaction between electrons is expected to yield an LL with $g < 1$ (refs 11, 12). For a finite-length tube or rope, the Luttinger parameter g is given by:

$$g = \left[1 + \frac{2U}{\Delta}\right]^{-1/2} \tag{1}$$

where U is the charging energy of the tube and Δ is the single-particle level spacing (the two one-dimensional sub-bands of the nanotube are assumed to be non-degenerate). From previous measurements and theoretical estimates[9,10] $U/\Delta \approx 6$, yielding an expected Luttinger parameter $g_{\text{theory}} \approx 0.28$.

The tunnelling of an electron into an LL is dramatically different from tunnelling into Fermi liquid. For a Fermi liquid, an energy-independent tunnelling amplitude is expected. This yields a temperature- and bias-independent tunnelling conductance. For a clean LL, on the other hand, the tunnelling amplitude is predicted to vanish as a power law in the energy of the tunnelling electron. This leads to a power-law variation of G with T at small biases ($eV \ll k_BT$);

$$G(T) \propto T^{\alpha} \tag{2}$$

or, with V at large biases ($eV \gg k_BT$):

$$dI/dV \propto V^{\alpha} \tag{3}$$

The exponent of these power laws depends on the number of one-dimensional channels[18] and on whether the electron tunnels into the bulk or the end of the LL. For a SWNT with four conducting modes at E_F, the exponents are[11,12]:

$$\alpha_{\text{end}} = (g^{-1} - 1)/4 \tag{4a}$$

$$\alpha_{\text{bulk}} = (g^{-1} + g - 2)/8 \tag{4b}$$

Using equations (1) and (4), we obtain $\alpha_{\text{end}}(\text{theory}) = 0.65$ and $\alpha_{\text{bulk}}(\text{theory}) = 0.24$.

To compare these theoretical predictions for tunnelling into an isolated nanotube through a single barrier to the experimental data obtained for ropes connected by two contacts, we must make two assumptions. First, we assume that transport in the rope is dominated by a single metallic tube, as discussed previously. Preliminary theoretical studies (L.B. and C. Kane, manuscript in preparation) of ropes composed of SWNTs with a relatively small fraction of metallic tubes support this assumption. These studies find that the only significant inter-tube coupling is electrostatic. Such an interaction will introduce extra screening of the Coulomb interaction but, because of the weak (logarithmic) dependence of g on the screening length, the LL predictions are essentially unchanged. Second, we assume that the tunnel resistances into and out of the tube are the dominent resistances in the system. The circuit thus consists of two tunnel junctions in series, with the current response of each junction described by equations (1)–(4). We note that the voltage drop across the highest-impedance junction will be some fraction γ of the total applied bias V, where $1/2 \leq \gamma \leq 1$. If the barriers are equal, the voltage will divide equally between these junctions and $\gamma = 1/2$. Alternatively, if the resistance of one junction dominates, $\gamma = 1$.

With these assumptions, the approximate power-law behaviour as a function of T or V observed in Figs 2 and 3 then follows from equations (1)–(4). The predicted values of the exponents are in good agreement with the experimental values. This agreement may be somewhat fortuitous owing to the experimental uncertainty in the value of U/Δ and complexities associated with the screening of the Coulomb interaction by the metallic leads[11,12]. Nevertheless, the measurements are described both qualitatively and quantitatively by LL theory. Power-law behaviour in T is observed up to 300 K in the bulk-contacted samples, indicating that nanotubes are LLs even at room temperature.

At present, we do not understand the origins of the high-energy saturation observed in the end-contacted tubes. One possibility is that, at high energies, electrons can tunnel in both directions and hence the end-contacted tubes behave as bulk-contacted tubes, with a correspondingly lower exponent. Further experiments are necessary to clarify this issue.

The LL theory makes an additional prediction for this system. The differential conductance for a single tunnel junction is given by a universal scaling curve[19,20]:

$$\frac{dI}{dV} = AT^{\alpha}\cosh\left(\gamma\frac{eV}{2k_BT}\right)\left|\Gamma\left(\frac{1+\alpha}{2} + \gamma\frac{ieV}{2\pi k_BT}\right)\right|^2 \tag{5}$$

where $\Gamma(x)$ is the gamma function, γ is the constant introduced earlier that takes into account the voltage division between the two tunnel junctions, and A is an arbitrary constant. This equation assumes that the leads are at $T = 0$ K. For leads at a finite temperature, dI/dV is given by the convolution of equation (5) and the derivative of the Fermi distribution: $df/dE = (1/4k_BT)\text{sech}^2(\gamma eV/2k_BT)$.

If the above scaling relation is correct, it should be possible to collapse the data at different temperatures onto a single universal curve. To do this, the measured dI/dV at each temperature was divided by T^{α} and plotted against eV/k_BT, as shown in Figs 3a and b. For both geometries, the scaled conductance is constant as eV/k_BT approaches zero, but increases when eV/k_BT is significantly greater than one. The data collapse quite well onto a universal curve for the bulk-contacted device over the entire bias range (Fig. 3a). For the end-contacted device, the data deviate from power-law behaviour for biases $V > 30$ mV, as discussed previously. This is reflected in Fig. 3b in a roll-off that occurs at lower values of eV/k_BT as the temperature is increased.

The solid lines in Fig. 3a and b are a plot of the curve obtained by fitting equation (5) (convolved with df/dE) to the data, with γ as a fitting parameter. The theory fits the scaled data reasonably well, especially for the bulk-contacted tube, and yields $\gamma = 0.5 \pm 0.1$ and $\gamma = 0.6 \pm 0.1$ for the bulk-contacted and end-contacted tubes, respectively. Given the associated experimental uncertainty, these values fall within the allowable range ($0.5 < \gamma < 1$) for two barriers in series.

Taken as a whole, the data shown in Figs 2 and 3 provide strong evidence that the electrons in metallic carbon nanotubes constitute an LL. Future work will test other predictions of this theory, such as tunnelling between LLs in end-to-end[1] and in crossed geometries[21]. □

Received 2 July; accepted 1 December 1998.

1. Fisher, M. P. A. & Glazman, A. *Mesoscopic Electron Transport* (Kluwer Academic, Boston, 1997).
2. Tarucha, S., Honda, T. & Saku, T. Reduction of quantized conductance at low temperatures observed in 2 to 10 μm-long quantum wires. *Solid State Commun.* **94,** 413–418 (1995).
3. Yacoby, A. *et al.* Nonuniversal conductance quantization in quantum wires. *Phys. Rev. Lett.* **77,** 4612–4615 (1996).
4. Milliken, F. P., Umbach, C. P. & Webb, R. A. Indications of a Luttinger liquid in the fractional quantum Hall regime. *Solid State Commun.* **97,** 309–313 (1996).
5. Chang, A. M., Pfeiffer, L. N. & West, K. W. Observation of chiral Luttinger behavior in electron tunneling into fractional quantum Hall edges. *Phys. Rev. Lett.* **77,** 2538–2541 (1996).
6. Grayson, M. *et al.* Continuum of chiral Luttinger liquids at the fractional quantum Hall edge. *Phys. Rev. Lett.* **80,** 1062–1065 (1998).
7. Wildoer, J. W. G. *et al.* Electronic structure of atomically resolved carbon nanotubes. *Nature* **391,** 59–62 (1998).
8. Odom, T. W., Huang, J., Kim, P. & Lieber, C. M. Atomic structure and electronic properties of single-walled carbon nanotubes. *Nature* **391,** 62–64 (1998).
9. Bockrath, M. *et al.* Single-electron transport in ropes of carbon nanotubes. *Science* **275,** 1922–1925 (1997).
10. Tans, S. J. *et al.* Individual single-wall carbon nanotubes as quantum wires. *Nature* **386,** 474–477 (1997).
11. Egger, R. & Gogolin, A. Effective low-energy theory for correlated carbon nanotubes. *Phys. Rev. Lett.* **79,** 5082–5085 (1997).
12. Kane, C., Balents, L. & Fisher, M. P. A. Coulomb interactions and mesoscopic effects in carbon nanotubes. *Phys. Rev. Lett.* **79,** 5086–5089 (1997).
13. Cobden, D. H. *et al.* Spin splitting and even–odd effects in carbon nanotubes. *Phys. Rev. Lett.* **81,** 681–684 (1998).
14. Tans, S. J., Devoret, M. H., Groeneveld, R. J. A. & Dekker, C. Electron–electron correlations in carbon nanotubes. *Nature* **394,** 761–764 (1998).
15. Grabert, H. & Devoret, M. H. *Single Charge Tunneling: Coulomb Blockade Phenomena in Nanostructures* (Plenum, New York, 1992).
16. Kane, C. L. & Mele, E. J. Size, shape, and low energy electronic structure of carbon nanotubes. *Phys. Rev. Lett.* **78,** 1932–1935 (1997).
17. Bezryadin, A., Verschueren, A. R. M., Tans, S. J. & Dekker, C. Multiprobe transport experiments on individual single-wall carbon nanotubes. *Phys. Rev. Lett.* **80,** 4036–4039 (1998).
18. Matveev, K. A. & Glazman, L. I. Coulomb blockade of tunneling into a quasi-one-dimensional wire. *Phys. Rev. Lett.* **70,** 990–993 (1993).
19. Fisher, M. P. A. & Dorsey, A. Dissipative quantum tunneling in a biased double-well system at finite temperatures. *Phys. Rev. Lett.* **54,** 1609–1612 (1985).
20. Grabert, H. & Weiss, U. Quantum tunneling rates for asymmetric double-well systems with ohmic dissipation. *Phys. Rev. Lett.* **54,** 1605–1608 (1985).
21. Komnik, A. & Egger, R. Nonequilibrium transport for crossed Luttinger liquids. *Phys. Rev. Lett.* **80,** 2881–2884 (1998).

Acknowledgements. We thank S. Louie, M. Cohen, D-h. Lee, A. Zettl and A. Georges for discussions. This work was supported by DOE (Basic Energy Sciences, Materials Sciences Division, the sp^2 Materials Initiative). L.B. was supported by the NSF.

Correspondence and requests for materials should be addressed to P.L.M. (mceuen@socrates.berkeley.edu).

The nature of the hydrated excess proton in water

Dominik Marx*, Mark E. Tuckerman†, Jürg Hutter* & Michele Parrinello*

* *Max-Planck-Institut für Festkörperforschung, Heisenbergstrasse 1, 70569 Stuttgart, Germany*

† *Department of Chemistry and Courant Institute of Mathematical Sciences, New York University, 4 Washington Place, New York, New York 10003, USA*

Explanations for the anomalously high mobility of protons in liquid water began with Grotthuss's idea[1,2] of 'structural diffusion' nearly two centuries ago. Subsequent explanations have refined this concept by invoking thermal hopping[3,4], proton tunnelling[5,6] or solvation effects[7]. More recently, two main structural models have emerged for the hydrated proton. Eigen[8,9] proposed the formation of an $H_9O_4^+$ complex in which an H_3O^+ core is strongly hydrogen-bonded to three H_2O molecules. Zundel[10,11], meanwhile, supported the notion of an $H_5O_2^+$ complex in which the proton is shared between two H_2O molecules. Here we use *ab initio* path integral[12–14] simulations to address this question. These simulations include time-independent equilibrium thermal and quantum fluctuations of all nuclei, and determine interatomic interactions from the electronic structure. We find that the hydrated proton forms a fluxional defect in the hydrogen-bonded network, with both $H_9O_4^+$ and $H_5O_2^+$ occurring only in the sense of 'limiting' or 'ideal' structures. The defect can become delocalized over several hydrogen bonds owing to quantum fluctuations. Solvent polarization induces a small barrier to proton transfer, which is washed out by zero-point motion. The proton can consequently be considered part of a 'low-barrier hydrogen bond'[15,16], in which tunnelling is negligible and the simplest concepts of transition-state theory do not apply. The rate of proton diffusion is determined by thermally induced hydrogen-bond breaking in the second solvation shell.

Simulating an excess proton in liquid bulk water has proved to be immensely challenging. Based on the efforts of numerous groups, many insights into the microscopic nature of proton hydration and diffusion have been deduced[17–31,38]. Structural diffusion[2] as a dynamical process was first 'seen' in microscopic detail in an *ab initio* molecular dynamics study of D^+ in D_2O (ref. 23). It was seen that proton diffusion does not occur via hydrodynamic Stokes diffusion of a rigid complex, but via migration of a structural defect due to a continual interconversion between covalent and hydrogen bonds. Solvent fluctuations modulate the proton transfer barrier and preselect a migration path. The rate-limiting step is the fluctuation-induced breakage of a hydrogen bond between the first and second solvation shell of H_3O^+, which reduces the coordination number of a water molecule in the first solvation shell[23]. It was subsequently suggested that quantum effects could potentially be important for the rattling of the proton in the hydrogen bond[24], but it has recently been shown that this depends sensitively on a qualitatively correct model for the interactions[27].

The quantum-mechanical particle density 'snapshots' from the present simulations of the hydrated proton give a pictorial realization of the structural diffusion process. Initially, the defect is localized as an $H_9O_4^+$ structure possessing an H_3O^+ core that donates three hydrogen bonds to neighbouring water molecules (Fig. 1a). In the second frame (Fig. 1b), one of the three protons of the H_3O^+ core migrates along its hydrogen bond and forms an $H_5O_2^+$ complex, in which this proton becomes equally shared between two water molecules. As the transfer is completed, an $H_9O_4^+$ complex is formed once again, but now centred on a neighbouring core molecule (Fig. 1c). The onset of further migration is shown in Fig. 1d, where the defect converts into another $H_5O_2^+$ configuration. Overall (Fig. 1a–d), the structural defect is displaced over a distance corresponding to approximately twice the average water–water distance, that is, about 5 Å. Each individual particle, however, moves by only a fraction of an ångström.

The controversial details of this process can be revealed by examination of the two-dimensional distribution $P(\delta, R_{OO})$ of the displacement coordinate $\delta = R_{O_aH} - R_{O_bH}$ of a given proton relative to the instantaneous hydrogen-bond centre and the corresponding bond distance R_{OO}. (See Fig. 1 legend for nomenclature.) For the analysis to be as unbiased as possible, we begin by including all O_aHO_b triples, that is, all hydrogen bonds present in the periodic sample. This distribution (not shown) is characterized by two prominent peaks around $(\delta, R_{OO}) \approx (\pm 0.9, 2.8)$ Å arising from the hydrogen bonds of bulk water but is manifestly non-zero around $|\delta| \approx 0$ Å. This supports the existence of centrosymmetric complexes, in which the proton is equally shared between two water molecules, and thereby opposes a description solely in terms of H_3O^+ or $H_9O_4^+$ complexes and/or proton transfer entirely associated with tunnelling.

The analysis can be refined by excluding 'irrelevant' hydrogen bonds in a two-step procedure. First, the $H_3O_a^+$ defect site is located, and only its three O_aHO_b triples are taken into account. Then, from these three triples, the hydrogen bond with the smallest $|\delta|$ is selected, an intuitive choice based on events of the type in Fig. 1. This second step focuses on the 'most active proton', that is, the one